XI International Conference on Computational Plasticity. Fundamentals and Applications
COMPLAS XI
E. Oñate, D.R.J. Owen, D. Peric and B. Suárez (Eds)

# COMPUTATIONAL MODELLING OF PROGRESSIVE FAILURE OF COMPOSITE MATERIALS AND STRUCTURES INCLUDING PLASTICITY EFFECTS

**EVGENY V. MOROZOV*, JINGFEN CHEN, KRISHNAKUMAR SHANKAR**

*School of Engineering and Information Technology
University of News South Wales at the Australian Defence Force Academy
Northcott Drive, 2600 Canberra ACT, Australia
e-mail: e.morozov@adfa.edu.au, web page: http://www.unsw.adfa.edu.au

**Key words:** Progressive Failure Analysis, Plasticity Effects, Composite Materials, Return Mapping Algorithm

**Abstract.** The paper is concerned with the development and verification of the computational algorithm enabling the progressive failure simulation that takes into account plasticity effects in addition to the damage progression to be performed for composite materials and structures.

The numerical approach is based on the combined elastoplastic damage model that accounts for the irreversible strains caused by plasticity effects and material properties degradation due to the damage initiation and development. The strain-driven implicit integration procedure is developed using equations of continuum damage mechanics, plasticity theory and includes the return mapping algorithm. A tangent operator that is consistent with the integration procedure is derived to ensure a computational efficiency of the Newton-Raphson method in the finite element analysis. The algorithm is implemented in ABAQUS as a user-defined subroutine. Prediction of the damage initiation in the laminated composite takes into account various failure mechanisms making use of Hashin's failure criterion. The plasticity effects in composite material are modelled using the approach developed by C. T. Sun and J. L. Chen.

The efficiency of the modelling approach and computational procedure is verified using the analysis of the progressive failure of composite laminates made of carbon fibre reinforced plastic and subjected to in-plane uniaxial tensile loading. It has been shown that the predicted results agree well with the experimental data.

## 1 INTRODUCTION

Laminated composite materials are widely used in aerospace, civil engineering, military vehicles, marine and many other industries due to their high strength and stiffness to weight ratios, good fatigue resistance and high energy absorption capacity. In many

applications, the progressive failure analysis of composite laminates is required to predict their mechanical behaviour under various loadings.

The development of an appropriate constitutive model for fibre reinforced composite materials normally involves the consideration of their mechanical response prior to the initiation of damage, the prediction of damage initiation and the modelling of postfailure behaviour. Continuum damage mechanics (CDM) provides a tractable framework for modelling damage initiation and development, as well as stiffness degradation. It is based on mesoscale, where a laminate is regarded as consisting of orthotropic plies. Several material models using continuum damage mechanics have been reported in literature [1–6]. Most of the CDM-based material approaches are based on elastic-damage models which are suitable for modelling the mechanical behaviour of elastic-brittle composites that do not exhibit noticeable nonlinearity or irreversible strains prior to the initiation of damage development. However, they may be insufficient in describing the nonlinear or plastic behaviour that some thermoset or thermoplastic composites might exhibit under transverse and/or shear loading. For example, research undertaken by Xiao [7] shows that material models that do not take into account the plastic features of composites failures might underestimate the energy absorbtion capacity of composite structures.

In addition to plasticity effects, material properties deterioration under loading is another significant feature of composite laminates. Defects such as fibre rupture, matrix cracks, fibre/matrix debonding developing in a ply do not lead to the collapse of a laminate immediately as they come up. These defects can accumulate gradually within the laminates. As a consequence, the material properties degrade progressively. Thus, the consideration of postfailure behaviour is important for an accurate prediction of failure loads.

Physically, the nonlinearity and/or irreversible deformations of fibre reinforced composites stem from the various mechanisms, such as the nonlinearity of each individual constituents, damage accumulation resulting from fibre or matrix cracking, and fibre/matrix interface debonding. Drucker [8] has proposed that such micromechanical phenomena can be described macroscopically within the framework of the plasticity theory. In combined plasticity and damage theories, the plastic strain represents all the irreversible deformations including those caused by microcracks. This approach is adopted in this study using an equivalent form of Sun and Chen plastic model [9]. The Hashin's failure criterion [10] is adopted to characterize the damage initiation and development.

Once damage initiates in the material, local stresses are redistributed in the undamaged area. As a result, the effective stresses in the undamaged area are higher than the nominal stresses in the damaged material. Plasticity is assumed to be developed in the undamaged area of the damaged material. So the effective stresses are used in the plastic model. Since the nominal stresses in the postfailure branch of the stress-strain curves decrease with the increase in strain, the use of these stresses in the failure criteria does not provide the prediction for further damage growth. Thus, the effective stresses are also applied in the Hashin's failure criteria.

## 2 ELASTOPLASTIC DAMAGE CONSTITUTIVE MODEL

The constitutive model is presented for an elementary orthotropic ply and consists of a plastic part which describes the plastic behaviour of composites under transverse and/or shear loading, failure criteria that are used to predict the thresholds for damage initiation and growth, and damage evolution laws that account for the development of damage.

### 2.1 Stress-strain relationship

Damage affects the behaviour of fibre-reinforced composite materials considerably. Material properties, such as elastic moduli and Poisson's ratio, degrade due to damage accumulation and growth. These effects are taken into account by introducing damage variables in the stiffness matrix using the CDM-based approaches. For example, the relation between the nominal stress and effective stress under uniaxial loading is given as

$$\sigma = (1-d)\bar{\sigma} \tag{1}$$

where $\sigma = P/A_0$ is the Cauchy nominal stress ($P$ is the normal internal force applied to the resisting surface, $A_0$ is the original area), $\sigma = P/A_{\text{eff}}$ is the effective stress ($A_{\text{eff}}$ is the effective resisting area of the damaged surface).

For composite materials exhibiting plasticity response, the total strain tensor $\boldsymbol{\varepsilon}$ is decomposed into the elastic and plastic strain parts $\boldsymbol{\varepsilon}^e$ and $\boldsymbol{\varepsilon}^p$ as

$$\boldsymbol{\varepsilon} = \boldsymbol{\varepsilon}^e + \boldsymbol{\varepsilon}^p \tag{2}$$

where the plastic strain $\boldsymbol{\varepsilon}^p$ represents all the irreversible deformations including those caused by microcracks.

According to the continuum damage mechanics theory, the stress-strain relationships for the damaged and undamaged composite materials are written in the following forms:

$$\boldsymbol{\sigma} = \mathrm{S}(d) : \boldsymbol{\varepsilon}^e; \quad \bar{\boldsymbol{\sigma}} = \mathrm{S}_{\mathbf{0}} : \boldsymbol{\varepsilon}^e \tag{3}$$

where bold-face symbols are used for variables of tensorial character and symbol (:) denotes inner product of two tensors with double contraction, e.g. $(\mathrm{S}(d) : \boldsymbol{\varepsilon}^e)_{ij} = \mathrm{S}(d)_{ijkl}\boldsymbol{\varepsilon}^e_{kl}$, where the summation convention is applied to the subscripts; $\boldsymbol{\sigma}$, $\bar{\boldsymbol{\sigma}}$ are the Cauchy nominal stress tensor and effective stress tensor (both are the second order tensors); $\mathrm{S}_{\mathbf{0}}$ is the fourth-order constitutive tensor for linear-elastic undamaged unidirectional laminated composite; $\mathrm{S}(d)$ is the one for the associated damaged material. The explicit form of $\mathrm{S}_{\mathbf{0}}$ is determined by elasticity theory for orthotropic materials. The form of the $\mathrm{S}(d)$ adopted in this model is similar to that presented by Matzenmiller et al. [2]

$$\mathrm{S}(d) = \frac{1}{D}\begin{bmatrix} (1-d_1)E_1^0 & (1-d_1)(1-d_2)\nu_{21}^0 E_1^0 & 0 \\ (1-d_1)(1-d_2)\nu_{12}^0 E_2^0 & (1-d_2)E_2^0 & 0 \\ 0 & 0 & D(1-d_3)G_{12}^0 \end{bmatrix} \tag{4}$$

where $D = 1 - (1 - d_1)(1 - d_2)\nu_{12}^0\nu_{21}^0$, $d_1$, $d_2$, $d_3$ denote damage developed in the fibre and transverse directions, and under shear (they are scalar damage variables that remain constant throughout the ply thickness); $E_1^0$, $E_2^0$, $G_{12}^0$ and $\nu_{12}^0$, $\nu_{21}^0$ are the elastic moduli and Poisson's ratios of undamaged unidirectional composite laminae.

In order to track the different failure mechanisms, namely, matrix microcraking and fibre rupture developed in the composite ply under tensile and compressive stresses, the damage variables are given as follows:

$$d_1 = \begin{cases} d_{1t} & \text{if } \sigma_1 \geq 0 \\ d_{1c} & \text{if } \sigma_1 < 0 \end{cases} \qquad d_2 = \begin{cases} d_{2t} & \text{if } \sigma_2 \geq 0 \\ d_{2c} & \text{if } \sigma_2 < 0 \end{cases} \tag{5}$$

where $d_{1t}$, $d_{1c}$ denote damage developments caused by tension/compression in the fibre direction, and, $d_{2t}$, $d_{2c}$ denote damage developments caused by tension/compression in the transverse direction.

It is assumed that the shear stiffness reduction results from the fibre and matrix cracking. To take this into account, the corresponding damage variable $d_3$ is expressed as:

$$d_3 = 1 - (1 - d_6)(1 - d_{1t}) \tag{6}$$

where $d_6$ represents the damage effects on shear stiffness caused by matrix cracking.

As mentioned before, all the irreversible deformations are represented by the plastic strain $\boldsymbol{\varepsilon}^p$. These effects are allowed for by the plastic model which includes the yield criterion, plastic flow rule, hardening variable flow rule, and the hardening law.

### 2.2 Plastic model

In the damaged materials, internal forces are resisted by the effective area. Thus, it is reasonable to assume that plastic deformation occurs in the undamaged area of the damaged composites. According to this, the plastic flow rule and hardening law are expressed in terms of effective stresses $\bar{\boldsymbol{\sigma}}$, equivalent plastic strain $\tilde{\varepsilon}^p$, and equivalent stress $\tilde{\sigma}$, which are based on the effective stress space concept.

The plastic yield function is given by:

$$F(\bar{\sigma}, \tilde{\varepsilon}^p) = F^p(\bar{\sigma}) - \kappa(\tilde{\varepsilon}^p) = 0 \tag{7}$$

where $F^p$ is the plastic potential; $\kappa$ is the hardening parameter which depends on the plastic deformations and is expressed in terms of equivalent plastic strain $\tilde{\varepsilon}^p$.

Due to its simplicity and accuracy, an equivalent form of the one-parameter plastic potential for plane stress condition proposed in [9] is adopted in this study to describe the irreversible strains exhibited by composites under transverse and/or shear loading:

$$F(\bar{\boldsymbol{\sigma}}, \tilde{\varepsilon}^p) = \sqrt{\frac{3}{2}(\bar{\sigma}_2^2 + 2a\bar{\sigma}_3^2)} - \tilde{\sigma}(\tilde{\varepsilon}^p) = 0 \tag{8}$$

where $a$ is a material parameter which describes the level of plastic deformation developed under shear loading compared to the transverse loading, $\bar{\sigma}_2$ is the effective stress in the

transverse direction, $\bar{\sigma}_3$ is the effective in-plane shear stress, and $\tilde{\sigma}(\tilde{\varepsilon}^p)$ is the isotropic hardening law for composites materials. Selecting the plastic criterion in the form of Eq.(8) improves efficiency and accuracy of the computational algorithm.

The equivalent stress is expressed in terms of $\bar{\sigma}_2$ and $\bar{\sigma}_3$ as follows [9]:

$$\tilde{\sigma} = \left[\frac{3}{2}(\bar{\sigma}_2^2 + 2a\bar{\sigma}_3^2)\right]^{\frac{1}{2}} \tag{9}$$

Assuming the associated plastic flow rule for composite materials, the plastic strain rate $\dot{\boldsymbol{\varepsilon}}^p$ is expressed as:

$$\dot{\boldsymbol{\varepsilon}}^p = \dot{\lambda}^p \partial_{\bar{\boldsymbol{\sigma}}} F \tag{10}$$

where $\dot{\lambda}^p \geq 0$ is a nonnegative plastic consistency parameter; hereafter $\partial_x y = \partial y / \partial x$.

Substituting Eq.(8) into Eq.(10), the following explicit form of plastic strain rate is derived:

$$\begin{bmatrix} \dot{\varepsilon}_1^p \\ \dot{\varepsilon}_2^p \\ \dot{\varepsilon}_3^p \end{bmatrix} = \dot{\lambda}^p \partial_{\bar{\boldsymbol{\sigma}}} F = \dot{\lambda}^p \begin{bmatrix} 0 \\ \frac{3}{2} \frac{\bar{\sigma}_2}{\sqrt{\frac{3}{2}(\bar{\sigma}_2^2 + 2a\bar{\sigma}_3^2)}} \\ \frac{3a\bar{\sigma}_3}{\sqrt{\frac{3}{2}(\bar{\sigma}_2^2 + 2a\sigma_3^2)}} \end{bmatrix} \tag{11}$$

In a similar fashion, the associated hardening rule is also assumed for the equivalent plastic strain rate and is presented as follows:

$$\dot{\tilde{\varepsilon}}^p = \dot{\lambda}^p h^p = \dot{\lambda}^p \partial_{\tilde{\varepsilon}^p} F \tag{12}$$

where $h^p$ defines the evolution direction of the equivalent plastic strain.

The equivalent plastic strain rate can be obtained from the equivalence of the rates of the plastic work per unit volume $W^p$

$$\dot{W}^p = \bar{\boldsymbol{\sigma}} : \dot{\varepsilon}^p = \tilde{\sigma} \dot{\tilde{\varepsilon}}^p \tag{13}$$

Substituting Eq.(11) and Eq.(9) into Eq.(13), the following relation is derived

$$\dot{\tilde{\varepsilon}}^p = \dot{\lambda}^p \tag{14}$$

It follows from the comparison of Eq.(12) and Eq.(14) that the value of $h^p$ is unity. Note that this result does not hold if the original quadratic form of the Sun and Chen yield criterion is adopted [9]. As a result, the application of the original yield criterion involves more computational efforts in the integration procedure. The current approach based on the use of Eq.(8) is free from this deficiency.

For the sake of simplicity, an isotropic hardening law expressed in terms of effective plastic strain $\tilde{\varepsilon}^p$ is adopted in this study. The following formulation of the isotropic hardening law proposed by Sun and Chen [9] is used to represent the equivalent stress versus equivalent strain hardening curve:

$$\kappa(\tilde{\varepsilon}^p) = \tilde{\sigma}(\tilde{\varepsilon}^p) = \beta(\tilde{\varepsilon}^p)^n \tag{15}$$

where $\beta$ and $n$ are coefficients that fit the experimental hardening curve. These parameters together with the material parameter $a$ are determined using an approach based on the linear regression analyses of the off-axis tensile tests performed on the unidirectional composite specimens [9, 11].

### 2.3 Damage model

#### 2.3.1 Damage initiation and propagation criteria

In order to predict the initiation and propagation of each intralaminar failure of the material and evaluate the effective stress state, the loading functions are adopted in the form of Hashin's failure criteria [10]. The damage initiation and propagation criteria $f_I$ are presented in the following form:

$$f_I(\phi_I, r_I) = \phi_I - r_I \leq 0 \quad I = \{1t, 1c, 2t, 2c, 6\} \tag{16}$$

where $\phi_I$ is the loading function and $r_I$ is the damage threshold corresponding to each failure mechanism. The damage threshold $r_I$ controls the size of the expanding damage surface and depends on the loading history. The damage development in the material initiates when $\phi_I$ exceeds the initial damage threshold $r_{I,0}$. Further damage growth occurs when the value of $\phi_I$ in the current stress state exceeds $r_I$ in the previous loading history. The damage variable $d_6$ represents the damage effect on shear stiffness due to matrix fracture caused by a combined action of transverse and shear stresses. However, the compressive transverse stress has beneficial effects on the matrix cracking. Thus, it is reasonable to assume that the damage effects are governed by the tensile matrix cracking only, i.e. $f_6$=$f_{2t}$.

According to Hashin's failure criteria, the loading functions for different failure mechanisms are given as:

$$\begin{aligned}
\phi_{1t} &= \left(\frac{\bar{\sigma}_1}{X_t}\right)^2 && (\bar{\sigma}_1 \geq 0) \quad \text{(tensile fibre damage mode)} \\
\phi_{1c} &= \left(\frac{\bar{\sigma}_1}{X_c}\right)^2 && (\bar{\sigma}_1 < 0) \quad \text{(compressive fibre damage mode)} \\
\phi_{2t} &= \left(\frac{\bar{\sigma}_2}{Y_t}\right)^2 + \left(\frac{\bar{\sigma}_3}{S_c}\right)^2 && (\bar{\sigma}_2 \geq 0) \quad \text{(tensile matrix damage mode)} \\
\phi_{2c} &= \left(\frac{\bar{\sigma}_2}{Y_c}\right)^2 + \left(\frac{\bar{\sigma}_3}{S_c}\right)^2 && (\bar{\sigma}_2 < 0) \quad \text{(compressive matrix damage mode)}
\end{aligned} \tag{17}$$

where $X_t$ and $X_c$ are the tensile and compressive strengths in fibre direction; $Y_t$ and $Y_c$ are the transverse tensile and compressive strengths; $S_c$ is the shear strength.

Once the damage initiation is predicted, the evolution of damage variable $d_I$ is determined by the damage flow rule and the damage evolution law.

### 2.3.2 Damage evolution

Under damage loading (i.e. when Eq.(16) is converted to equality) the damage consistency condition $\dot{f}(\phi_I, r_I) = 0$ is satisfied. Then the following expressions for damage thresholds $r_I$ can be derived:

$$r_I = \max\{1, \max\{\phi_I^\tau\}\} \quad I = \{1t, 1c, 2t, 2c, 6\} \quad \tau \in [0, t] \tag{18}$$

Since damage is irreversible, the damage evolution rate should satisfy the following condition: $\dot{d}_I \geq 0$. The exponential damage evolution law is adopted for each damage variable and expressed in the following form [12]

$$d_I \quad = 1 - \frac{1}{r_I}\exp(A_I(1 - r_I)) \quad I = \{1t, 1c, 2t, 2c, 6\} \tag{19}$$

where $A_I$ is parameter that defines the exponential softening law. This parameter is determined by regularizing the softening branch of the stress-strain curve to ensure the computed damage energy within an element is constant and thus avoid mesh dependency. The regularization is based on the Bazant's crack band theory [13]. According to this, the damage energy dissipated per unit volume $g_I$ for uniaxial loading or shear is related to the critical strain energy release rate $G_{I,c}$ along with the characteristic length of the finite element $l^*$ as follows

$$g_I = \frac{G_{I,c}}{l^*} \quad I = \{1t, 1c, 2t, 2c, 6\} \tag{20}$$

The critical strain energy release rates $G_{2t,c}$ and $G_{6,c}$ in this work are referred to as the intralaminar mode I and mode II fracture toughness parameters. The parameter $G_{2c,c}$ is the intralaminar model I fracture toughness under compression. The parameters $G_{1t,c}$ and $G_{1c,c}$ correspond to the mode I fracture energies of fibre breakage under tension and compression, respectively. The ways of identification of these parameters including the characteristic length $l^*$ are described in [4, 14].

The damage energy dissipated per unit volume for uniaxial stress conditions is obtained from the integration of the damage energy dissipation during the damage process:

$$g_I = \int_0^\infty Y_I \dot{d}_I \mathrm{d}t; \quad Y_I = -\frac{\partial \psi}{\partial d_I}; \quad \psi = \frac{1}{2}\boldsymbol{\sigma} : \boldsymbol{\varepsilon} \quad I = \{1t, 1c, 2t, 2c, 6\} \tag{21}$$

where $Y_I$ is the damage energy release rate, $\dot{d}_I$ is the rate of damage development defined as $\dot{d}_I = \mathrm{d}d_I/\mathrm{d}t$, and $\psi$ is the Helmhotlz free energy. Equating Eq.(20) and Eq.(21), the parameter $A_I$ is calculated numerically.

The loading/unloading stress strain curves of the present elastoplastic damage model are shown in Figure 1. Under longitudinal loading, the material is assumed to exhibit linear elastic brittle behaviour and the irreversible strain is not developed. Beyond the damage initiation, the elastic modulus $E_1$ is assumed to degrade gradually. It is assumed, that under transverse and shear loading, the irreversible deformations are exhibited prior to the damage initiations, however, there is no stiffness degradation. Beyond the damage initiation points, both irreversible deformations and stiffness degradations are taken into account.

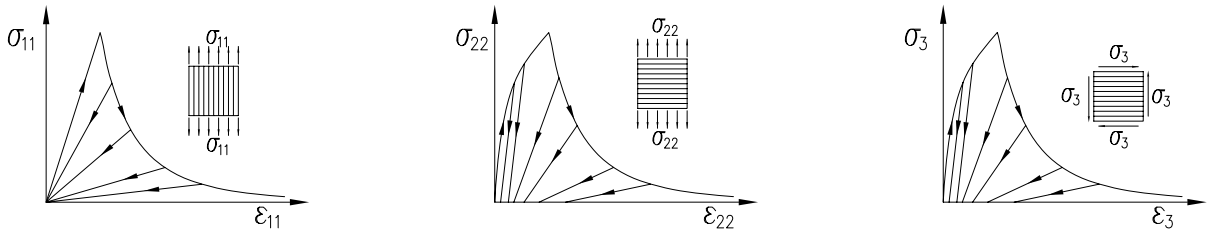


(a) longitudinal (b) transverse (c) in-plane shear

**Figure 1**: Loading/unloading stress-strain curves.

## 3 NUMERICAL IMPLEMENTATION

The proposed elastoplastic damage material model is embedded in Abaqus/Standard finite element software package using the user-defined subroutine UMAT. The numerical integration algorithms updating the Cauchy nominal stresses and solution-dependent state variables are derived as well as the tangent matrix that is consistent with the numerical integration algorithm ensuring the quadratic convergence rate of the Newton-Raphson method in the finite element procedures.

### 3.1 Integration algorithm

The solution of the nonlinear inelastic problem under consideration is based on the incremental approach and is regarded as strain driven. The loading history is discretized into a sequence of time steps $[t_n, t_{n+1}], n \in \{0, 1, 2, 3...\}$ where each step is referred to as the $(n+1)$th increment. Driven by the strain increment $\triangle\varepsilon$, the discrete problem in the context of backward Euler scheme for the elastoplastic damage model can be stated as: for a given variable set $\{\boldsymbol{\varepsilon}_n, \boldsymbol{\varepsilon}^p_n, \tilde{\varepsilon}^p_n, \bar{\boldsymbol{\sigma}}_n, \boldsymbol{\sigma}_n, r_{I,n}, d_{I,n}\}$ at the beginning of the $(n+1)$th increment, find the updated variable set $\{\varepsilon^p_{n+1}, \tilde{\varepsilon}^p_{n+1}, \bar{\boldsymbol{\sigma}}_{n+1}, \boldsymbol{\sigma}_{n+1}, r_{I,n+1}, d_{I,n+1}\}$ at the end of the $(n+1)$th increment. The updated stresses and solution-dependent state variables are stored at the end of the $(n+1)$th increment and are passed on to the user subroutine UMAT at the beginning of the next increment.

The effective stress strain relationship Eq.(3), the yield criterion Eq.(8), the associated plastic flow rule Eq.(10), and the hardening power law Eq.(15) constitute the nonlinear plastic constitutive material model. Using the backward Euler implicit integration procedure, the corresponding integration algorithm is formulated as follows:

$$\begin{aligned}
\boldsymbol{\varepsilon}_{n+1} &= \boldsymbol{\varepsilon}_n + \triangle\boldsymbol{\varepsilon} \\
\boldsymbol{\varepsilon}^p_{n+1} &= \boldsymbol{\varepsilon}^p_n + \triangle\lambda^p_{n+1}\partial_{\bar{\boldsymbol{\sigma}}_{n+1}} F^p_{n+1} \\
\tilde{\varepsilon}^p_{n+1} &= \tilde{\varepsilon}^p_n + \triangle\lambda^p_{n+1} \\
\bar{\boldsymbol{\sigma}}_{n+1} &= \mathrm{S}_0 : (\boldsymbol{\varepsilon}_{n+1} - \boldsymbol{\varepsilon}^p_{n+1}) \\
F_{n+1} &= F(\bar{\boldsymbol{\sigma}}_{n+1}, \tilde{\varepsilon}^p_{n+1}) \leq 0
\end{aligned} \tag{22}$$

where $\triangle\lambda^p_{n+1} = \dot{\lambda}^p_{n+1}\triangle t$ is the increment of the plastic consistency parameter.

The closest point return mapping algorithm is employed to solve this nonlinear coupled system. The solutions $\{\varepsilon^p_{n+1},\ \tilde{\varepsilon}^p_{n+1},\ \bar{\boldsymbol{\sigma}}_{n+1}\}$ are the converged values at the end of the $(n+1)$th increment. They ensure that upon yielding, the determined stress state lies on the yield surface and prevent the drift from the yield surface due to the unconverged solutions obtained from the forward Euler integration scheme.

The nonlinear system Eq.(22) is linearized and solved iteratively using the Newton-Raphson scheme. The iterations are performed until the final set of state variables $\{\bar{\boldsymbol{\sigma}}^{(k+1)}_{n+1}, \varepsilon^{p,(k+1)}_{n+1}, \tilde{\varepsilon}^{p,(k+1)}_{n+1}\}$ in the $(k+1)$th iteration fulfil the yield criterion $F(\bar{\boldsymbol{\sigma}}^{(k+1)}_{n+1}, \tilde{\varepsilon}^{p,(k+1)}_{n+1}) \leq$ TOL, where TOL is the error tolerance which is set to $1 \times 10^{-6}$.

Substituting the effective stresses $\bar{\boldsymbol{\sigma}}_{n+1}$ into the damage model, the damage variables are updated. According to Eq.(3), the Cauchy stresses are calculated as $\boldsymbol{\sigma}_{n+1} = \mathrm{S}(d_{n+1}) : \boldsymbol{\varepsilon}^e_{n+1}$.

### 3.2 Consistent tangent stiffness matrix

The consistent tangent matrix for the proposed constitutive model is derived in the following form:

$$\frac{\mathrm{d}\boldsymbol{\sigma}_{n+1}}{\mathrm{d}\varepsilon_{n+1}} = [M_{n+1} + \mathrm{S}(d_{n+1})] : C_0 : \mathrm{S}^{\mathrm{alg}}_{n+1} \tag{23}$$

in which $M_{n+1}$ can be presented in the indicial form as follows:

$$M_{ik}|_{n+1} = \left.\frac{\partial \mathrm{S}(d)_{ij}\varepsilon^e_j}{\partial \varepsilon^e_k}\right|_{n+1} = \varepsilon^e_j \frac{\partial \mathrm{S}(d)_{ij}}{\partial d_p}\frac{\partial d_p}{\partial r_t}\frac{\partial r_t}{\partial \phi_t}\frac{\partial \phi_t}{\partial \bar{\boldsymbol{\sigma}}_q}\left.\frac{\partial \bar{\boldsymbol{\sigma}}_q}{\partial \varepsilon^e_k}\right|_{n+1} \quad p,q,k = \{1,2,3\};\ t = \{1,2\} \tag{24}$$

where matrix $M_{ik}$ of is asymmetric. This results in the asymmetry of the consistent tangent matrix of the elastoplastic damage model. In Eq.(23), $C_0$ is the compliance matrix of the undamaged composite materials and $\mathrm{S}^{\mathrm{alg}}_{n+1}$ is the consistent tangent matrix for the discrete plastic problem Eq.(22). The latter is expressed as:

$$\mathrm{S}^{\mathrm{alg}}_{n+1} = \frac{\mathrm{d}\bar{\boldsymbol{\sigma}}_{n+1}}{\mathrm{d}\boldsymbol{\varepsilon}_{n+1}} = \tilde{\mathrm{S}}_{n+1} - \frac{(\tilde{\mathrm{S}}_{n+1} : \partial_{\bar{\boldsymbol{\sigma}}} F^p_{n+1}) \otimes \{\tilde{\mathrm{S}}_{n+1} : \partial_{\bar{\boldsymbol{\sigma}}} F_{n+1}\}}{\partial_{\bar{\boldsymbol{\sigma}}} F_{n+1} : \tilde{\mathrm{S}}_{n+1} : \partial_{\bar{\boldsymbol{\sigma}}} F^p_{n+1} - \partial_{\tilde{\varepsilon}^p} F_{n+1}} \tag{25}$$

where $\tilde{\mathrm{S}}_{n+1} = (C_0 + \triangle\lambda^p_{n+1}\partial^2_{\bar{\boldsymbol{\sigma}}\bar{\boldsymbol{\sigma}}} F^p_{n+1})^{-1}$, $\triangle\lambda^p_{n+1}$ is the increment of plastic consistent parameter in the $(n+1)$th increment, $(\otimes)$ denotes a tensor product.

### 3.3 Viscous regularization

Numerical simulations based on the implicit procedures, such as Abaqus/Standard, and the use of material constitutive models that are considering strain softening and material stiffness degradation often abort prematurely due to convergence problems. In order to alleviate these computational difficulties and improve convergence, a viscous regularization scheme has been implemented in the following form [5]:

$$\dot{d}^v_m = \frac{1}{\eta}(d_m - d^v_m), \quad m = \{1,2,3\} \tag{26}$$

where $d_m$ is the damage variable obtained as described previously, $d_m^v$ is the regularized viscous damage variable, and $\eta$ is the viscosity coefficient.

The corresponding regularized consistent tangent matrix is derived as:

$$\left.\frac{\mathrm{d}\boldsymbol{\sigma}_{n+1}}{\mathrm{d}\boldsymbol{\varepsilon}_{n+1}}\right|_v = [M_{n+1}^v + \mathrm{S}(d_{n+1}^v)] : \mathrm{C}_0 : \mathrm{S}_{n+1}^{\mathrm{alg}}; \quad M_{n+1}^v = M(d_{n+1}^v) \cdot \frac{\triangle t}{\eta + \triangle t} \tag{27}$$

## 4 NUMERICAL RESULTS AND VERIFICATIONS

Numerical simulations of the progressive failure of 12 sets of T300/1034-C carbon/epoxy composite laminates with different geometries and different layups, containing a central circular hole and subjected to uniform in-plane tensile loading, were performed using the numerical procedure presented in previous sections. Three material layups were considered, namely, $[0/(\pm 45)_3/90_3]_s$, $[0/(\pm 45)_2/90_5]_s$, $[0/(\pm 45)_1/90_7]_s$ with the material properties listed in Table 1 along with other model parameters used in the finite element simulations. The geometry of the laminates is illustrated in Figure 2(a). The hole diameters $D$ and widths of the laminates $W$ are listed in Table 2. The predicted failure stresses $\sigma_u$ ($\sigma_u = P_u/(WH)$, $P_u$ is the failure load) were compared with the experimental results reported by Chang et al. [15] along with the numerical results obtained by Chang and Chang [16], Tan [17], and Maimí [4]. As shown in Table 2, the results demonstrates that the predicted failure stresses correlate well with the test data and generally more accurate in comparison with predictions made by Chang [16], and Tan [17]. Figure 2(b) illustrates the comparison of the load versus displacement curves corresponding to the cases labeled ✠ in Table 2.

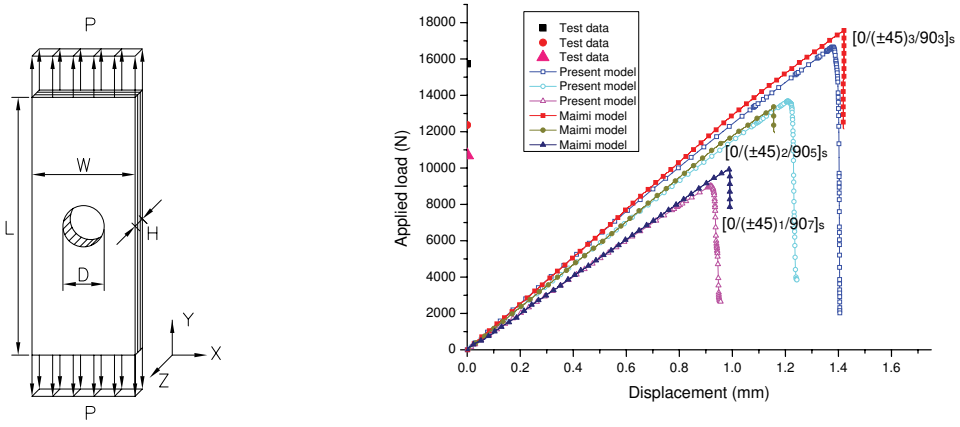


(a) (b)

Figure 2: (a) Geometry of the laminate ($L = 203.2\ mm$, $H = 2.616\ mm$); (b) load vs. displacement curves.

**Table 1**: Material properties of T300/1034-C and plastic model parameters

| $E_1^0$ | $E_2^0$ | $G_{12}^0$ | $\nu_{12}^0$ | $X_t$ | $X_c$ | $Y_t$ | $Y_c$ | $S_c$ |
|---|---|---|---|---|---|---|---|---|
| 146.8 GPa | 11.4 GPa | 6.1 GPa | 0.3 | 1730.0 MPa | 1379.0 MPa | 66.5 MPa | 268.2 MPa | 58.7 MPa |
| $G_{1t,c}$ | $G_{1c,c}$ | $G_{2t,c}$ | $G_{2c,c}$ | $G_{6,c}$ | $a$ | $\beta$ | $n$ | $\eta$ |
| 89.83 N/mm | 78.27 N/mm | 0.23 N/mm | 0.76 N/mm | 0.46 N/mm | 1.25 | 567.9092 | 0.272405 | 0.0002 |

**Table 2**: Comparison of the tensile failure stresses of T300/1034-C carbon/epoxy laminates

| | | | | Failure stress $\sigma_u$ MPa | | | | | Error % | | | |
|---|---|---|---|---|---|---|---|---|---|---|---|---|
| Lay-up | Label | D (mm) | W (mm) | Present | Chang † | Tan † | Maimí | Test data | Present | Chang | Tan | Maimí |
| $[0/(\pm45)_3/90_3]_s$ | a | 3.175 | 19.05 | 293.07 | 227.53 | 275.75 | — | 277.17 | 5.74 | -17.91 | -0.5 | — |
| $[0/(\pm45)_3/90_3]_s$ | b | 6.35 | 38.1 | 252.22 | 206.84 | 275.79 | — | 256.48 | -1.66 | -19.35 | 7.53 | — |
| $[0/(\pm45)_3/90_3]_s$ | c | 3.175 | 12.7 | 269.05 | 206.84 | 262.00 | — | 226.15 | 18.97 | -8.54 | 15.85 | — |
| $[0/(\pm45)_3/90_3]_s$ | d | 6.35 | 25.4 | 238.30 ✱ | 179.26 | 248.21 | 263.1✱ | 235.80 ✱ | 1.06 | -23.98 | 5.26 | 11.6 |
| $[0/(\pm45)_2/90_5]_s$ | a | 3.175 | 19.05 | 239.13 | 193.05 | 186.16 | — | 236.49 | 1.12 | -18.37 | -21.28 | — |
| $[0/(\pm45)_2/90_5]_s$ | b | 6.35 | 38.1 | 214.30 | 172.37 | 186.16 | — | 204.08 | 5.00 | -15.54 | -8.78 | — |
| $[0/(\pm45)_2/90_5]_s$ | c | 3.175 | 12.7 | 216.28 | 165.47 | 172.37 | — | 177.88 | 21.58 | -6.98 | -3.10 | — |
| $[0/(\pm45)_2/90_5]_s$ | d | 6.35 | 25.4 | 205.83 ✱ | 151.68 | 158.58 | 200.1✱ | 185.47 ✱ | 10.98 | -18.22 | -14.50 | 7.7 |
| $[0/(\pm45)_1/90_7]_s$ | a | 3.175 | 19.05 | 171.03 | 144.79 | 227.53 | — | 190.98 | -10.45 | -24.19 | 19.13 | — |
| $[0/(\pm45)_1/90_7]_s$ | b | 6.35 | 38.1 | 150.36 | 124.11 | 227.53 | — | 158.58 | -5.18 | -21.74 | 43.48 | — |
| $[0/(\pm45)_1/90_7]_s$ | c | 3.175 | 12.7 | 154.96 | 124.11 | 213.74 | — | 134.45 | 15.25 | -7.69 | 58.97 | — |
| $[0/(\pm45)_1/90_7]_s$ | d | 6.35 | 25.4 | 135.67 ✱ | 103.42 | 199.95 | 148.2✱ | 159.96 ✱ | -15.19 | -35.34 | 25.00 | -7.4 |

† Chang and Chang [16] and Tan [17].
✱ The load vs. displacement curves of these two sets of simulations are shown in Figure 2(b)

## 5 CONCLUSIONS

An elastoplastic damage constitutive model capable of simulating progressive failure of composite laminates has been developed. The model takes into account various failure mechanisms and plasticity effects. The corresponding numerical method based on the finite element formulation was developed and applied to the solution of the related nonlinear problems. The approach has been verified using numerical simulations of the progressive failure of the various laminates containing the central through hole. It has been shown that the proposed solution procedure provides sufficiently accurate predictions of the failure loads for the composite laminates made from the carbon fibre reinforced plastic.

## REFERENCES

[1] Ladeveze, P. and Le Dantec, E. Damage modelling of the elementary ply for laminated composites. *Compos. Sci. Technol.* (1992) **43**(3) : 257–267.

[2] Matzenmiller, A., Lubliner, J. and Taylor, R. L. A constitutive model for anisotropic damage in fiber-composites. *Mech. Mater.* (1995) **20**(2):125–152.

[3] Maimí, P., Camanho, P. P., Mayugo, J. A. and Dávila, C. G. A continuum damage model for composite laminates: Part I - Constitutive model. *Mech. Mater.* (2007) **39**(10):897–908.

[4] Maimí, P., Camanho, P. P., Mayugo, J. A. and Dávila, C. G. A continuum damage model for composite laminates: Part II - Computational implementation and validation. *Mech. Mater.* (2007) **39**(10):909–919.

[5] Lapczyk, I. and Hurtado, J. A. Progressive damage modeling in fiber-reinforced materials. *Composites Part A* (2007) **38**(11):2333–2341.

[6] Van Der Meer, F. P. and Sluys, L. J. Continuum models for the analysis of progressive failure in composite laminates. *J. Compos. Mater.* (2009) **43**(20):2131–2156.

[7] Xiao,X. Modeling energy absorption with a damage mechanics based composite material model. *J. Compos. Mater.* (2009) **43**(5):427–444.

[8] Drucker, D. C. Yielding, flow and failure. In C. T. Herakovich, editor, *Inelastic behaviour of composite materials* (1975) volume 13 of *AMD*, 1–15. Houston, Texas.

[9] Sun, C. T. and Chen, J. L. A simple flow rule for characterizing nonlinear behavior of fiber composites. *J. Compos. Mater.* (1989) **23**(10):1009–1020.

[10] Hashin, Z. Failure criteria for unidirectional fiber composites. *J Appl. Mech-T ASME*(1980) **47**(2):329–334.

[11] Winn, V. M. and Sridharan, S. An investigation into the accuracy of a one-parameter nonlinear model for unidirectional composites. *J. Compos. Mater.* (2001) **35**(16):1491–1507.

[12] Faria, R., Oliver, J. and Cervera, M. A strain-based plastic viscous-damage model for massive concrete structures. *Int. J. Solids Struct.*(1998) **35**(14):1533–1588.

[13] Bazant, Z. and Oh, B. Crack band theory for fracture of concrete. *Mater. Struct.* (1983) **16**:155–177.

[14] Pinho, S. T. *Modelling failure of laminated composites using physically-based failure models.* PhD thesis. Department of Aeronautics, Imperial College, London, UK. (2005).

[15] Chang, F. K., Scott, R. A. and Springer, G. S. Strength of bolted joints in laminated composites. Technical Report AFWAL-TR-84-4029, Air Force Wright Aeronautical Laboratories, (1984).

[16] Chang, F. K. and Chang, K. Y. A progressive damage model for laminated composites containing stress concentrations. *J. Compos. Mater.* (1987) **21**:834–55

[17] Tan, S. C. A progressive failure model for composite laminates containing openings. *J. Compos. Mater.* (1991) **25**(5):556–577